Dual mechanism model for fluid particle breakup in the entire turbulent spectrum

Received: 7 December 2018 | Revised: 28 February 2019 | Accepted: 15 March 2019

DOI: 10.1002/aic.16600

Dual mechanism model for fluid particle breakup in the entire turbulent spectrum

Mohsen Karimi | Ronnie Andersson

Department of Chemistry and Chemical Engineering, Chalmers University of Technology, Gothenburg, Sweden

Correspondence
Mohsen Karimi, Department of Chemistry and Chemical Engineering, Chalmers University of Technology, SE-41296 Gothenburg, Sweden.
Email: mohsenk@chalmers.se

Funding information
Swedish Research Council, Grant/Award Number: 621-2013-5964

Abstract

This work provides an in-depth understanding of different breakup mechanisms for fluid particles in turbulent flows. All the disruptive and cohesive stresses are considered for the entire turbulent energy spectrum and their contributions to the breakup are evaluated. A new modeling framework is presented that bridges across turbulent subranges. The model entails different mechanisms for breakup by abandoning the classical limitation of inertial models. The predictions are validated with experiments encompassing both breakup regimes for droplets stabilized by internal viscosity and interfacial tension down to the micrometer length scale, which covers both the inertial and dissipation subranges. The model performance ensures the reliability of the framework, which involves different mechanisms. It retains the breakup rate for inertial models, improves the predictions for the transition region from inertia to dissipation, and bridges seamlessly to Kolmogorov-sized droplets.

KEYWORDS
mathematical modeling, multiphase flow, process, simulation, turbulence

1 | INTRODUCTION

The size distribution of fluid particles within a continuous medium is of vital importance for different industrial applications. In multiphase processes, knowledge of size distribution determines the rate of momentum, heat and mass transport. The mathematical framework commonly used to tackle this problem is population balance modeling, which requires closure terms for the breakup and coalescence of the dispersed fluid particles.[1,2] The present work concentrates on the breakup mechanisms of fluid particles in turbulent flows.

The pioneering models for breakup were formulated by Rayleigh in the nineteenth century for jet flows, and considered dynamic stresses and surface tension.[3] Taylor,[4,5] on the other hand, has shown the relevance of viscous stresses for droplet distortions when the droplets are very small or when the continuous phase is highly viscous. Balancing the deforming and stabilizing stresses, Hinze has proposed a formulation for the maximum stable droplet diameter (d_{max}) for dispersion in turbulent flows.[6] The above advancements have paved the way for further developments in the field. Typically, the ratio between counteracting stresses acting on fluid particles represents a dimensionless number that indicates the probable breakup mechanism. For instance, when inertia is the principal cause of breakup, a critical Weber number is quantified, and the break up takes place above this number; examples can be found in Reference [7–9]. The other scenario is the definition of a critical Capillary number (i.e., the ratio of viscous stress over surface stresses) for viscous laminar flows.[10–12] Although the dimensionless numbers are a relevant means for interpreting the breakup process, relying on dimensionless numbers to explain the complicated physical phenomenon that occurs during the breakup in turbulent multiphase systems is too simplistic.[13,14] Thus, later breakup models are inclined toward the dynamics of bubble or droplet collision with a turbulent structure, which has a limited length scale. Extensive research has been conducted on developing breakup models.

Refer to References [15–23] for some of the most used models, and refer to References [24–26] for review articles.

The conventional strategy in previous models has assumed that the inertia force due to the interaction of vortices and droplets is the main reason for the breakup of fluid particles. The interaction is mathematically formulated as a frequency term multiplied by a probability function, or the breakup rate itself is modeled as the inverse of breakage time. However, most models account only for the inertial subrange of isotropic turbulent flows. Therefore, they are unable to provide reasonable predictions of the breakup rate for droplets with diameters outside the inertial subrange and require high *Re* numbers. For example, for high viscosity emulsions in stirred vessels, it is likely that droplets experience a high dissipation rate of turbulent kinetic energy in the vicinity of the rotational zone, which may lead to droplets smaller than the Kolmogorov length scale (i.e., η). The monotonous increase in the functional form of conventional models, however, yields either negligible breakup rates or extremely large values for very small or very large mother droplets. This can be translated into the fact that the breakup mechanism for all mother droplets is similar, regardless of their diameters, in accordance with the turbulent energy spectrum. Furthermore, the viscous stresses acting on droplets due to the mean velocity gradient of the continuous phase and the internal viscosity of the fluid particles as a stabilizing stress are not often considered in classical breakup models, except for a few works that have addressed the importance of these stresses during breakup.[26–29] For instance, the models proposed by Håkansson et al[29] and Solsvik et al[26] include viscous stresses using the critical *We* and *Ca* numbers. The models, however, rely on calibration factors, and their performance have not been evaluated. Nevertheless, the turbulent viscous shear stress and the internal viscosity of droplets for the sub-Kolmogorov scale could be the determinant factors needed to understand breakup mechanisms. Table 1 summarizes the breakup models with regard to physical mechanisms and the subrange of the turbulent energy spectrum. The table shows that the turbulent inertia stress due to the turbulent structures of diameters within the inertial subrange has been the dominant theory of breakup modeling. Recently, a number of limited works have been published that include the possibility of breakup due to the turbulent inertia stress for the entire turbulent spectrum.[30–32] The validations in these works were carried out using rough estimations of turbulent properties. We have addressed this limitation by validating a new extended model for a realistic system in chemical engineering for inertial and dissipation subranges.[33] The methodology proposed in the present work connects the breakup mechanisms across the entire spectrum of turbulence and includes all the disruptive and cohesive stresses. For instance, the new methodology accounts for the effect of turbulent viscous shear and the stabilizing effect of internal viscosity for high viscosity multiphase systems where the Ohnesorge number is not negligible.

Later in this article, we will show through practical examples how different stresses contribute to the breakup. There is also notable interest in the formation of droplets with diameters comparable to the Kolmogorov scale from the industrial standpoint, since droplet size distribution governs the stability and the rheology of the final product. For instance, Hinze[6] has formulated the following expression for the maximum stable droplet diameter (d_{max}):

$$d_{max} \propto \left(\frac{\sigma}{\rho_c}\right)^{3/5} \varepsilon^{-2/5} \tag{1}$$

In later studies, the effect of droplet viscosity as a stabilizing term that counteracts the turbulent fluctuating velocity of the continuous phase is included in the definition of d_{max}.[34,35] Chen and Middleman[36] and Shinnar[28] have also proposed different proportionalities for the maximum stable droplet diameter for droplets with diameters smaller than the Kolmogorov length scale. Additional semiempirical models have been proposed in the literature to determine d_{max} in a fully turbulent flow under different disruptive and cohesive stresses.[37–41] The surfactant effect on reducing interfacial tension, which results in smaller bubble size distribution, has also been discussed by Ramezani et al.[42] What should be highlighted from the previous works on formulating equations for the maximum stable droplet diameter is that different breakup mechanisms occur in two distinct turbulent subranges (see Table 1). The first mechanism postulates that pressure fluctuation is the dominant disruptive stress compared to interfacial stress, whereas the viscous shear stress due to the velocity gradient in the continuous phase dictates the fragmentation phenomenon. The above classifications have also been verified with experimental evidences.[39,41,43,44] It has unanimously been concluded that inertia stress is the main reason for breakup when the diameter for the stable droplet is larger than the Kolmogorov length scale (i.e., $d_{max} > \eta$). On the other hand, $d_{max} < \eta$ specifies that the turbulent viscous stress characterizes the breakup in the dissipation subrange of turbulence. In practice, however, there is no distinct change in the Kolmogorov length scale, and this is, instead, a smooth transition around the value of η that must be captured by the kernel. The expressions proposed in the literature for the estimation of d_{max} lack generality, and experiments should be carried out to obtain the proportionality constants for the desired operational conditions. Although semiempirical formulations of stable droplet diameters provide some insights into the breakup

TABLE 1 Conceptual summary of breakup models with regard to physical mechanisms and turbulent subrange

	Turbulent subrange		Disruptive stress		Cohesive stress	
Breakup model	**Inertial**	**Dissipation**	**Turbulent inertia**	**Turbulent viscous shear**	**Interfacial**	**Internal viscous**
Classical[a] formulations[24–26]	✓	×	✓	×	✓	×
Recent works 2016[30–32] to 2018[33]	✓	✓	✓	×	✓	×
Current formulation	✓	✓	✓	✓	✓	✓

[a]Theoretical models based on the frequency of vortex-fluid particle collision and probability of successful breakup.

mechanism, there is no corresponding breakup rate model that captures the various breakup mechanisms. To the best of authors' knowledge, formulations of the breakup rate models do not account for the transition of breakup from the inertia to the viscous regime. Moreover, most of the semiempirical models for the maximum stable droplet diameters have approximated the velocity fluctuation term using the Kolmogorov formulation of the second-order structure function for the inertial subrange.[45] This evidently initiates errors when the droplet diameter falls outside the inertial subrange of turbulence (e.g., the viscous dominant breakup in the dissipation subrange).

The present work aims at enhancing the physical understanding of different breakup mechanisms for fluid particles and provides quantitative models that allow the calculation of breakup rates for both regimes. Through the analysis of disruptive and cohesive stresses, we determine their contributions to breakup rate, and we show how the conventional way, which does not include all the stresses for calculating breakup rates, is prone to erroneous predictions. Further, a breakup rate model is constructed that logically links the inertial and dissipation subranges of the turbulent energy spectrum. This model also takes into account the transition of breakup regimes from inertia dominant to viscous dominant. The modeling framework allows two mechanisms of breakup in fully turbulent systems, as the entire spectrum of turbulent energy is employed. In this way, the present limitation in the breakup rate models imposed by applying the inertial subrange is overcome. The new model is applied to estimate breakup rates, stable droplet sizes, and to validate model predictions with experimental measurements from the literature.

2 | MODEL DESCRIPTIONS

The breakup of a fluid particle in an isotropic turbulent flow depends on balancing the summation of disruptive stresses due to the continuous phase, with the summation of the interfacial tension and the internal viscous stress of the fluid particle. The magnitude of stresses varies significantly, according to continuous phase hydrodynamics, and the dispersed phase fluid properties and droplet size. These changes consequently alter the breakup probability. Therefore, it is important to address how the changes govern the breakup. For example, for low viscosity fluid particles, the turbulent inertia stress from the interaction between the vortex and the fluid particle deforms the mother droplet, whereas interfacial stress resists deformation. For such a system, the internal viscosity of a fluid particle as well as the viscous shear stress due to the mean flow velocity gradient can be safely omitted, as shown experimentally by Ashar et al.[46] On the other hand, the effect of turbulent viscous shear stress and the internal viscous stress for micron-sized droplets determine the breakup mechanism. It should be noted that the effect of surface additives on interfacial stress is not accounted for in the current work. This is similar to previous studies devoted to the development of breakup kernels for chemical engineering applications. In other words, the model determines application where the interfacial stress is quantified by Laplace stress. Table 2 summarizes the different stresses that influence the breakup process. The Greek letter ψ in the table is for the disruptive stresses with subscript *i* for inertia and *v* for viscous shear, whereas τ is the stabilizing stresses with subscript *i* for interfacial and *v* for internal viscosity effect. The continuous phase density and viscosity are defined by ρ_c and μ_c, while ρ_d and μ_d are for dispersed phase density and viscosity, respectively. The diameter of the fluid particle undergoing the breakup is defined as d_0, and σ indicates interfacial tension.

To close the equation set for stresses (i.e., Equations (2)–(5)), the functional forms of $u_\lambda, \bar{G}$ and τ_{ext} should be clarified. The term u_λ defines the mean turbulent fluctuating velocity for the vortex of the length scale λ, and it is approximated by the Kolmogorov second-order structure function $u_\lambda \approx \sqrt{\left\langle [\delta v]^2 \right\rangle(\lambda)} \approx \sqrt{2}(\varepsilon\lambda)^{1/3}$ classically for the inertial subrange of turbulence.[6,47–49] The validation of structure function through DNS data or experimental measurements remains an open question. However, its implicit validation can be traced by its application in breakup rate models.[7,21,50] The second unknown term, $\bar{G}$ in Table 2, is the local deformation rate imposed by the velocity gradient of vortices. The shear between the droplet and the turbulent structure caused by the velocity gradient is the main reason for the deformation. The velocity fluctuations at two points in the flow field are assessed by the structure function, which is the equivalent of the energy spectrum in spatial space, and it defines how the velocities at two points are correlated. Thus, the deformation rate can be modeled as $\bar{G} = \sqrt{\left\langle [\delta v]^2 \right\rangle(\lambda)}/\lambda$, and replacing the nominator with the Kolmogorov structure function yields an expression that is only valid for the inertial subrange of turbulence. The different methods of determining turbulent viscous stresses are explained further in Supporting Information. The magnitude of internal viscous stress is only substantial for small viscous droplets identified by $Oh > 1$. Therefore, care must be taken to apply the pertinent range of vortex sizes that exert kinetic energy on the fluid particle surface to the

TABLE 2 Disruptive and cohesive stresses for fluid particle breakup

Disruptive stress (kg/m·s^2)		Cohesive stress (kg/m·s^2)	
Turbulent inertia	**Turbulent viscous shear**	**Interfacial**	**Internal viscous**
$\psi_i = \frac{\rho_c}{2} u_\lambda^2$ (2)	$\psi_v = \mu_c \bar{G}$ (3)	$\tau_i = \frac{2\sigma}{d_0}$ (4)	$\tau_v = \frac{\mu_d}{d_0}\sqrt{\frac{\tau_{\text{ext}}}{\rho_d}}$ (5)

formulation of the external stress in Equation (5) (i.e., τ_{ext}). Thus, we have adopted the general form of external stress that reads as[35]:

$$\tau_{ext} = \rho_c \int_{\kappa_{min}}^{\kappa_{max}} E(\kappa) d\kappa \tag{6}$$

where $E(\kappa)$ is the turbulent energy spectrum, and κ_{min} and κ_{max} identify the effective range of wave numbers. This study assumes that the minimum effective size of turbulent structure is half of the Kolmogorov length scale, since below this limit the number density of vortices is negligible. Further, different limits have been exploited in the literature for the maximum effective size of turbulent structure, including, $3d_0$, $5d_0$, and $10d_0$.[21–23,51,52] In the present work, $\lambda/d_0 \le 10$ is employed as the upper limit of the vortex size. More details on the choice of integration bounds are provided in this section. Subsequently, the final form of the internal viscous stress for the sub-Kolmogorov scale depends on both the dispersed phase and continuous phase properties. It is important to note that, for high viscous droplets, breakup occurs after continuous stretching of the fluid particle. Thus, scaling the internal viscous stress with the diameter of a spherical droplet might lead to error. This approach has, however, been applied in previous investigations including the effect of internal viscosity for breakup rate models.[20,26,29] In this work, we compare three different shapes, including sphere, cylinder and prolate ellipsoid, to account for the deformed shape when determining internal viscous effects. Andersson and Andersson[53] have used high-speed imaging to observe sequences of deformed droplets. They found that the aspect ratio of the deformed droplet can be up to five times larger than the mother droplet. Thus, the aspect ratio of five for the cylinder and ellipsoid is assumed when estimating internal viscous stress.

TABLE 3 Analytical solution for the second-order structure function[32]

$$\left\langle [\delta v]^2 \right\rangle(\lambda) = \frac{4}{3} k \left[\frac{\lambda^2}{\lambda_d^2 + \lambda^2} \right]^{2/3} \{1 - [T_1(\lambda) + T_2(T_3(\lambda) T_4(\lambda) - T_5(\lambda))]\} \tag{7}$$

$$T_1(\lambda) = \frac{2}{[s(\lambda)]^2} F\left(\left(-\frac{1}{3} \right)^{1/2}, \left(\frac{3}{2} \right) \middle| \frac{[s(\lambda)]^2}{4} \right) \tag{8}$$

$$T_2 = 5.2\Gamma\left(\frac{2}{3} \right) \tag{9}$$

$$T_3(\lambda) = 27 \times 2^{1/3} [s(\lambda)]^{2/3} \Gamma\left(\frac{2}{3} \right) \tag{10}$$

$$T_4(\lambda) = \frac{1}{352\pi} F\left(\left(\frac{7}{3} \right)^{11/6}, \left(\frac{17}{6} \right) \middle| \frac{[s(\lambda)]^2}{4} \right) \tag{11}$$

$$T_5(\lambda) = \frac{2^{2/3}}{2\pi [s(\lambda)]^{2/3}} K_{4/3}(s(\lambda)) \tag{12}$$

$$s = \frac{\kappa\lambda}{C_L^{-1/2} \kappa L} \tag{13}$$

Note. And F, K and Γ are hypergeometric, Bessel, and gamma functions with $\lambda_d = (30)^{3/4}\eta$.

Recent advances in turbulence theory, improve the simplifying assumption that binds breakup only to the inertial subrange. Limited efforts have been made to extend the energy spectrum to cover dissipation, inertial and energy-containing subranges.[32,54–59] Solsvik and Jakobsen[32] have analytically solved the second-order structure function of Davidson[60] and added a semiempirical model, as suggested by Sawford and Hunt,[61] to formulate a model for the number density of vortices for the entire spectrum. They compared their approach with other formulations for the entire spectrum and concluded that the model works with reasonable accuracy for all *Re* numbers. The solution of the structure function is summarized in Table 3.

In order to mitigate the limitation of the inertial subrange assumption, Equation (7) was substituted in Equations (2), (3), and (6) to account for the entire spectrum of turbulence while performing stress analysis. However, for a practical computation and to justify the additional computational effort, this should be performed after identifying the turbulent properties of the flow. To indicate the various subranges of the turbulence, a viable option is the number density of vortices ($\dot{n}_\lambda$). The number density plot estimates the different length scales corresponding to the dissipation subrange, inertial subrange and the energy-containing subrange of turbulence. This allows determining where the mother droplet diameter is located with regard to the subrange of turbulence, and the Kolmogorov length scale, which in turn, governs the correct choice of formulation for the second-order structure function. In the proceeding analysis of the number density of vortices, we have applied the suggestion of Solsvik et al,[32,57] to extend the formulation by Pope[48] for turbulent energy for the entire spectrum that reads as:

$$\dot{n}_\lambda = \frac{48 \varepsilon^{2/3} \lambda^{-10/3} f_L\left(\frac{2\pi}{\lambda} L\right) f_\eta\left(\frac{2\pi}{\lambda}\eta\right)}{1.5 \times (2\pi)^{5/3} \left\{ \frac{4}{3} k \left[\frac{\lambda^2}{\lambda_d^2 + \lambda^2} \right]^{2/3} \{1 - [T_1(\lambda) + T_2(T_3(\lambda) T_4(\lambda) - T_5(\lambda))]\} \right\}} \tag{14}$$

$$f_L\left(\frac{2\pi}{\lambda}L\right) = \left\{\frac{\frac{2\pi}{\lambda}L}{\left[\left(\frac{2\pi}{\lambda}L\right)^2 + c_L\right]^{1/2}}\right\}^{5/3+p_0} \tag{15}$$

$$f_\eta\left(\frac{2\pi}{\lambda}\eta\right) = \exp\left\{-\beta\left(\left[\left(\frac{2\pi}{\lambda}\eta\right)^4 + c_\eta^4\right]^{1/4} - c_\eta\right)\right\} \tag{16}$$

where L is the integral length scale, the model constants are $p_0 = 2$, $\beta = 5.2$, and the last two unknown terms c_L and c_η are functions of the turbulent Reynold number (Re_L) reported by Reference [32,57]. In what follows, a breakup rate model is formulated that differentiates breakup mechanisms through stress analysis. The aim of the model is to address the current deficiency of a sound methodology for calculating specific breakup rate, when other stresses are more substantial than turbulent inertia stress. The model is constructed on the breakup rate model by Andersson and Andersson.[21] The choice of this modeling strategy is motivated by the fact that not only should an energy criterion be satisfied for the fluid particle to break, but it should also include a stress measure for the breakup of a fluid particle. The energy criterion is to overcome the energy barrier due to surface energy, whereas the stress criterion evaluates whether the disruptive stresses surpass the cohesive stresses. The functional form of this model includes an interaction frequency term ($\dot{\omega}(d_0,\lambda)$) times a probability function ($P(d_0,\lambda)$). This mathematical paradigm has proven to be feasible in terms of accuracy and computational requirements.[16,21,52] The original model was constructed for the inertial subrange, and consisted of only the turbulent inertia and interfacial stresses. The new model formulation, in contrast, includes the transition of breakup from the inertia-dominant regime to the viscous-dominant regime. It also covers the entire spectrum of turbulence, accounting for sub-Kolmogorov droplets in high viscosity emulsions. As it embodies all the stresses contributing to the deformation and stabilization of the fluid particle, it can be applied to seamlessly predict the breakup rate and the maximum stable diameter for bubbles or droplets. The model derivation stems from the general form of the specific breakup rate as suggested by Andersson and Andersson[21]:

$$\Omega_s(d_0) = \int_{\lambda_{\min}}^{\lambda_{\max}} \dot{\omega}(d_0,\lambda) \times P(d_0,\lambda) d\lambda \tag{17}$$

The breakup phenomenon described in Equation (17) is a statistically independent event. This means instead of assuming that turbulent structures bombard the fluid particle, the turbulent vortices independently interact with the fluid particle and there is no systematic accumulation of surface energy between the interactions. This has been also shown experimentally[21] and with high resolved simulations.[62] The former assumption (i.e., bombarding turbulent structures) necessitates the definition of an arbitrary swept volume for formulating the collision terms, while the latter conditions the deformation of the fluid particle on a physical energy criterion. In that, the interaction of the turbulent structure with fluid particle must be energetic enough that within the lifetime of turbulent vortex the fluid particle surface deforms. Moreover, this definition clarifies that the deformation of the droplet is not caused by the energy accumulation due to a series of vortices colliding with the surface. It has also been shown that the specific breakup rate is independent of the integration limits.[21] The integration bounds for Equation (17) have insignificant effects on the final breakup rate. This is explained by using physical criteria including stress and energy for the breakup probability. The two criteria are not met for the small vortices, while very large turbulent structures, even though they satisfy both criteria, have low number densities and long life-times, resulting in trivial contributions to the breakup. For the lower integration limit, we have explored $0.1\eta < \lambda_{\min} < \eta$, which shows no distinctive difference in the results. Furthermore, the reason for exploring a range for the lower integration limit is to consider sub-Kolmogorov droplets for emulsions, and how they interact with vortices around the Kolmogorov scale. In this way, the asymptotic behavior of the model close to the Kolmogorov size is clarified. In fact, for such vortices, the number density of turbulent structures decreases approximately by six to ten orders of magnitude for the range of η to 0.1η. Figure 1 shows the normalized cumulative plot of breakup rates for two different systems (water–dodecane and water–rapeseed oil). The details for these two systems are explained in Section 3. The figure shows that the model can provide the upper integration limit based on the contribution of different vortices. For instance, for the water–dodecane with a droplet diameter of 1 mm, vortices up to three times larger than the mother droplet are important, while for the rapeseed oil droplet of diameter 0.1 mm, vortices ten times larger than the droplet diameter contribute to the breakup.

The interaction frequency is modeled as the number density of vortices ($\dot{n}_\lambda$ in Equation (14)) interacting with a droplet of diameter d_0 for a limited time.

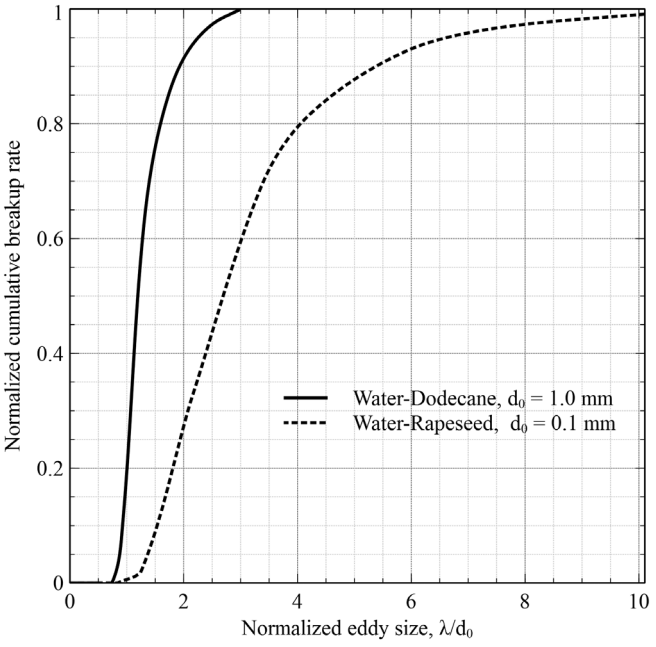

FIGURE 1 Normalized cumulative breakup rates for water–rapeseed oil[46] and water–dodecane[53]

$$\dot{\omega}(d_0,\lambda) = \dot{n}_\lambda \times \frac{\pi}{6} d_0^3 \times \frac{1}{t_i} \tag{18}$$

The time-scale t_i in Equation (18) is defined as:

$$t_i = \begin{cases} \left(\frac{\nu}{\varepsilon}\right)^{1/2} d_0 < \eta \\ \frac{\lambda^{2/3}}{\varepsilon^{1/3}} \; d_0 \geq \eta \end{cases} \tag{19}$$

The time scale has been modified in comparison to the original model comprising the Kolmogorov timescale for droplets with diameters smaller than the Kolmogorov length scale. The probability term in Equation (17) is described based on the dimensionless energy and stress criteria required for the breakup.

$$P(d_0,\lambda) = \exp\left(-\max\left(\chi_{\text{energy}},\chi_{\text{stress}}\right)\right) \tag{20}$$

The energy criterion in Equation (20) determines whether the available energy for the breakup can overcome the surface energy increase. The exponential form of the probability function has been suggested by Luo and Svendsen[16] and experimentally confirmed by Kuboi et al,[63]

$$\chi_{\text{energy}} = \frac{0.3\sigma\pi d_0^2}{\min\left[\rho_c \frac{\pi\lambda^3}{6} \frac{u_\lambda^2}{2}, d_0^2 \lambda \frac{\pi^2}{8} \rho_c u_\lambda^2\right]} \tag{21}$$

It should be noted that the structure function in the denominator of Equation (21) has been modified to include the entire spectrum of turbulence. The first term in the denominator of Equation (21) includes the average vortex energy for vortices smaller than the diameter of the mother droplet. The second term, on the other hand, estimates the energy of vortices larger than d_0; such an approach assures that the contributions of all vortices have been accounted for. In addition, the stress criterion has been updated to include all the stresses summarized in Table 2, and according to the system under investigation, their relevance are determined in the results for the breakup rate to allow seamless transition. Equation (22) has been introduced to update the stress criterion, and it comprises all the available disruptive and cohesive stresses. This can be interpreted that as a generalized indication that the constituent stresses for the breakup process have been balanced. Note that the linear summation of the stresses was inspired by previous work in high-viscosity droplets, where the internal viscous stress is added to the interfacial stress.[20,27,64,65] Alternatively, one can choose the maximum of the disruptive and cohesive stresses for calculating the balance between the stresses and predicting the stable droplet diameter. However, the linear summation was applied in this work to consistently account for all the stresses for the validation studies.

$$\chi_{\text{stress}} = \frac{\tau_i + \tau_v}{\psi_i + \psi_v} \tag{22}$$

The above concept of breakup modeling enables us to incorporate alternative breakup mechanisms by utilizing all the disruptive and cohesive stresses. It also accounts for the droplets smaller than the Kolmogorov length scale by estimating the structure function for the entire spectrum of turbulence and updating the associated timescale for the interaction frequency term. As a general guideline to use the modeling strategy, one should, as a first step, evaluate the number density of vortices. The analysis of the $\dot{n}_\lambda$ plot in conjunction with the Kolmogorov length scale is then compared to the range of available mother droplet diameters. The comparison identifies the correct expression for the second-order structure function to use. The next step is to perform stress calculation with the specific objective of pinpointing the crucial stresses (see Figure 2). The specific breakup rate that is coupled with the results of stress analysis and the number density of vortices are eventually calculated.

3 | RESULTS AND DISCUSSION

The main objective is to demonstrate that different physical phenomena are responsible for the breakup of fluid particles and that the model is capable of handling the different breakup mechanisms. This was achieved by employing the stress calculations and the entire turbulent spectrum for three characteristic experimental conditions. The conditions include model validation for the inertial subrange where the breakup rate measurements are available. The validation continues for the transition region between the inertial to the dissipation subrange by considering the breakup rate and the stable droplet diameters. Eventually, the breakup phenomenon was validated for the dissipation subrange by comparing the model predictions with the measurements of the maximum stable droplet diameters. The remainder of this section includes three subsections that explore the possible regions for breakup mechanisms, and the effective subrange of the turbulent energy spectrum (see Table 1). Before evaluating the model performance, it is important to understand how the choice of formulations for the second-order structure function can alter the magnitude of disruptive stresses and eventually the breakup mechanisms. Thus,

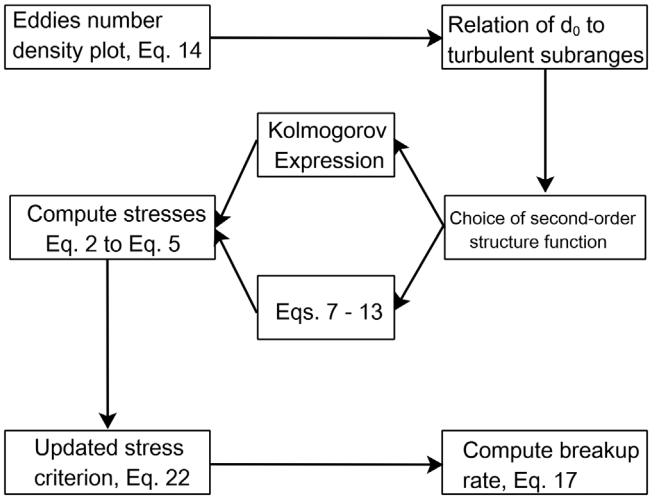

FIGURE 2 Schematic representation of calculations in the new breakup framework

an example of applying different formulae (the Kolmogorov expression and Equation (7) for the entire spectrum) was used to calculate the disruptive stresses.

Figure 3 shows the number density of vortices (Figure 3a) and the disruptive stresses (Figure 3b) for the emulsification of water–rapeseed oil in a rotor-stator mixer. The details of this system are reported in Reference [44]. The emulsion was a mixture of rapeseed oil with 65% (w/w) aqueous sugar solution as the dispersed phase following a power-law model for describing the rheological behavior of the emulsion. The continuous phase was water at 20°C. An emulsifier (Polysorbate 80) was used to suppress the effect of coalescence between the droplets, and the stable droplet diameters were measured at different impeller velocities. We have chosen the tip velocity of 23 m s^{-1}. Håkansson et al, applied empirical expressions for predicting the maximum stable diameters, and compared the outcomes with their measurements. They concluded that the dominant breakup mechanism was turbulent viscous fragmentation. This implied that the stress analysis was controlled by the viscous stresses.

The plot for the number density of vortices (Figure 3a) shows the inertial subrange of turbulence (where the two lines overlap) and the Kolmogorov length scale (η), which show the effective range of interest for droplet breakup (i.e., $d_0 = 5 \times 10^{-6}$ m < $\eta = 3.6 \times 10^{-5}$ m). Applying different formulations (i.e., inertial subrange and entire spectrum) initiates a large deviation on the number of interacting vortices for droplets with diameters outside the inertial subrange. The assumption is that a droplet interacts with vortices of a limited size range. The number of vortices with length scales smaller than the Kolmogorov is negligible, and large vortices only weakly contribute to breakup. Nevertheless, a sensitivity analysis of the limits of vortex sizes invariably showed that the final outcomes were not sensitive to these limits. In other words, the models filter out the effective size of vortices causing the breakup. Accordingly, the two disruptive stresses were calculated based on the length scales of different vortices. Figure 3b compares the magnitude of turbulent inertia (ψ_i) and viscous shear stresses (ψ_v), where the second-order structure function is approximated by the Kolmogorov formulation for the inertial subrange, and Equation (7) for the entire spectrum. It is evident from Figure 3 that using the Kolmogorov approximation for the structure function yields significant overpredictions for both inertia and viscous shear stresses for droplets with diameters inside the dissipation subrange of turbulence, and further away from the inertial subrange the difference is greater. The disruptive stresses, calculated with the two different formulations for the second-order structure function, show a maximum of two orders of magnitude difference, and the differences are minimized closer to the inertial subrange, which underlines the importance of correct formulation. For instance the observed trend for the viscous shear stress indicate large values for small vortices which correspond to the large values of turbulent vortex velocity using inertial subrange formulation. On the other hand, owing to the application of entire spectrum for the structure function the viscous shear stress for the entire spectrum shows smaller magnitudes that converge to the inertial subrange computations within the inertial subrange. The paramount importance of dissimilar formulae for the estimation of structure function is that they might lead to diverse interpretations of the breakup mechanism and, consequently, result in erroneous breakup rates. It should also be noted that, for this example, the magnitude of viscous shear stress is dominant and must be considered for the breakup rate model formulation. This is consistent with Håkansson et al,[44] who found, based on their empirical formulation, that the breakup was associated with turbulent viscous stresses. Yet, the breakup rate models available in the literature do not include the viscous shear stresses as one of the disruptive stresses that contribute to the breakup and cannot successfully be applied to predict the breakup rate.

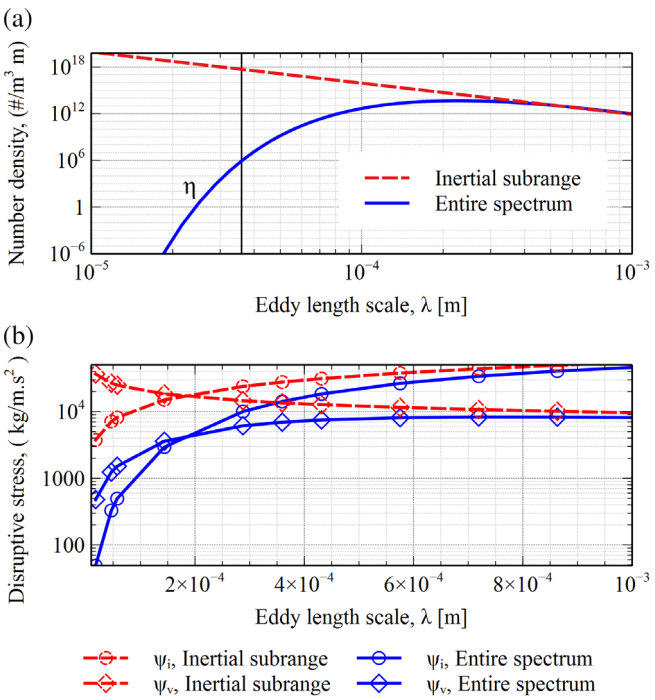

FIGURE 3 Comparison of inertial subrange and entire spectrum formulations (a) number density of vortices and (b) magnitude of disruptive stresses for sub-Kolmogorov scale [Color figure can be viewed at wileyonlinelibrary.com]

3.1 | Inertia stress—inertial subrange

This subsection starts by evaluating the different stresses employed for the specific breakup rates in a liquid–liquid system with mother droplet diameters well within the inertial subrange. Andersson and Andersson[21] have analyzed the number of both stable and unstable droplets in a multipurpose reactor for water–dodecane under a moderate Reynolds number (Integral scale *Re*, $Re_L = 889$, Taylor scale *Re*, $Re_\lambda = 77$). Figure 4 shows the disruptive (Figure 4a), cohesive (Figure 4b), and summation of different stresses (Figure 4c) for a dodecane droplet with a diameter of 1 mm. The Kolmogorov structure function, valid for the inertial subrange of turbulence, was applied for the stress analysis. The diameter of the dodecane droplet is larger than the Kolmogorov length scale ($\eta = 1.85 \times 10^{-5}$ m), and the turbulent inertia stress, caused by the interaction of turbulent vortices with

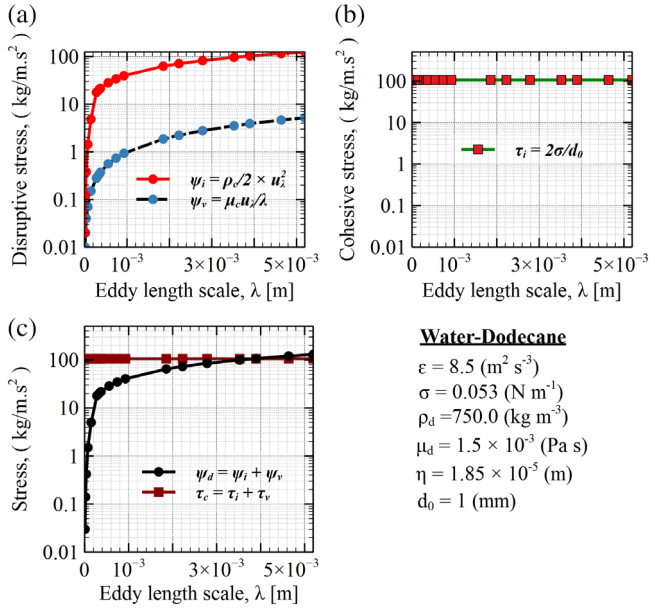

FIGURE 4 Disruptive and cohesive stresses calculated for water–dodecane system [Color figure can be viewed at wileyonlinelibrary.com]

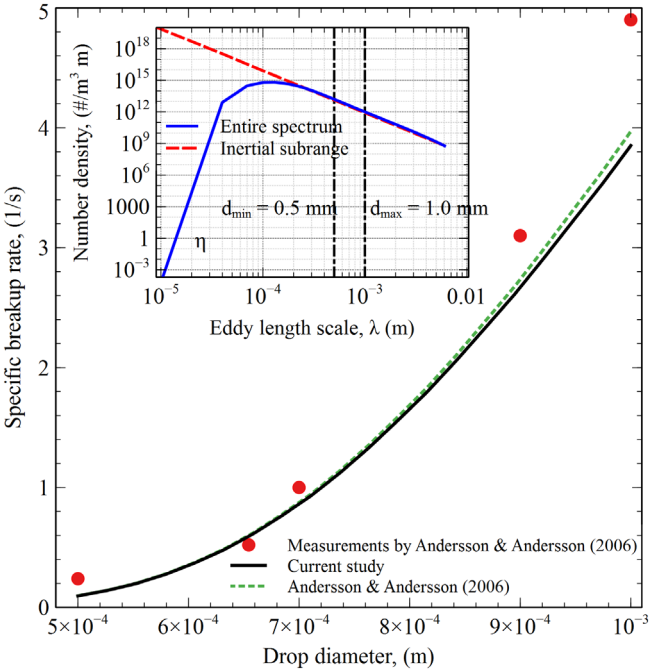

FIGURE 5 Validation of current breakup model for the inertial subrange with experiments by Andersson and Andersson[21] [Color figure can be viewed at wileyonlinelibrary.com]

the droplet, is expected to be the main cause for droplet deformation and breakup. Comparing the magnitude of ψ_i with ψ_v in Figure 4a confirms this theory. The stress due to the internal viscosity is insignificant (*Oh* = 0.01), and, therefore, interfacial tension is the only stress acting against the deformation of the droplet (Figure 4b). It is also interesting to note that the summation of stresses (Figure 4a,b) shows that the plot of cohesive stress intersects with the summation of disruptive stresses. In other words, the stress analysis suggests that breakup can occur for this particular droplet. The measurement of the breakup rate for the droplet of size 1.0 mm equals 4.9 s^{-1}, which ensures the consistency of the stress analysis approach for determining the breakup mechanism.

The stress analysis establishes that the turbulent inertia stress and the interfacial stress are the controlling factors for the breakup. Taking into account the prominent stresses, Figure 5 compares the numerical predictions of breakup rates using the new model and the original Andersson and Andersson model with the experimental data. The number density of vortices for the inertial and the entire spectrum have been plotted to show that the range of mother droplet diameters is within the inertial subrange (i.e., where the two lines overlap on the number density plot). The increasing trend of breakup rate with droplet size has been captured with both models, and there is good quantitative agreement between the measurements and the numerical predictions (maximum error < 20%). It is not surprising that the new model converges with the original model by Andersson and Andersson, since the latter is formulated for the inertial subrange of turbulence. In fact, the overlap of the two plots in Figure 5 further supports the idea that fluid particle breakup is controlled by the counteracting turbulent inertia and interfacial surface stresses (i.e., an inertia-dominant breakup mechanism).

3.2 | Inertia stress—transition from inertial to dissipation subrange

Turbulent inertia stress can be the prevailing disruptive stress for fluid particle breakup, with diameters stretching from the inertial subrange into the dissipation subrange of turbulence. This is the second relevant zone for the breakup phenomenon as shown in Table 1. The model in the transition zone is validated through a comparison of breakup rate predictions with direct measurements, and estimation of maximum stable droplet diameter by applying stress analysis. The raw experimental data were obtained from Ashar et al,[46] who performed measurements in a rotor-stator mixer with water as the continuous phase and rapeseed oil as the dispersed phase. The dissipation rates of turbulent kinetic energy were determined from PIV data using two different approaches that included subgrid scale dissipation (SGD) and intermediary eddy length scale (ILT).[66,67] The maximum difference between these two methodologies was found to be 35%. Given the number of stable and broken droplets in this experimental set, the Jackknife method was used to approximate the level of uncertainty for the breakup rate predictions. This method is based on leaving out one observation at a time to provide jackknife samples.[68] The resampling method then led to small error bars compared to the scale of the plots. Moreover, one must note that even though the high-speed imaging technique is a nonintrusive measurement method and does not disturb the flow, there is inherent uncertainties in representing a three-dimensional phenomenon by two-dimensional images. For instance, the deformation and fragmentation of droplets in unreachable zones from the camera might raise uncertainties in registering the breakup details such as time scales and number of fragments. There is also a coupling

between the accuracy of the measurements and the temporal and spatial resolutions of the experiments. In other words, the fastest breakup rate and the smallest fragments are constrained by the camera speed and resolution. The reason for choosing this multiphase system to validate of the current modeling framework is twofold. First, there is a data point toward the dissipation subrange of turbulence that reflects how the model performs in transition from the inertial subrange to the dissipation subrange. This system also enables validation of the model predictions with measurements of specific breakup rates. Figure 6 shows the validation procedure, including the plot of vortex number densities (Figure 6a), a stress analysis (Figure 6b) and a comparison of breakup rate predictions with experiments (Figure 6c). The number density plot shows the inertial subrange of turbulence, and the magnitude of the diameter of mother droplet. As shown in the figure, the smallest droplet size in this data set (i.e., d_{min} = 100 μm) is close to the dissipation subrange of turbulence, the diverging point in Figure 6a. The stress analysis for d_0 = 100 μm, shown in Figure 6b, imparts the importance of internal viscosity of droplets as a stabilizing component of the breakup process for this system with Oh = 1.6 (μ_d = 0.0699 kg m^{-1}s^{-1}). This component of the breakup process is usually neglected in most breakup models. The other essential message from the stress analysis is how the application of the entire turbulent energy spectrum can modify the magnitude of the turbulent inertia stress close to the dissipation subrange (i.e., d_0 = 100 μm). For instance, using the Kolmogorov structure function in Equation (2) to calculate turbulent inertia stress yields a disruptive stress that is approximately twice as large as that if the entire turbulent spectrum had been used, leading to excessive breakup rate. This large value of disruptive stresses translates to higher specific breakup rates, and might mislead the interpretation of the breakup mechanism. Figure 6c validates the breakup rates with the measurements, and it provides a comparison with the predictions of the original model by Andersson and Andersson.[21] The predictions by present model is qualitatively similar to the trend of experiments that are monotonically increasing with diameters, and, as shown, the current model is an overall improvement in the prediction of breakup rates compared to the original model by Andersson and Andersson. For the best case (the smallest mother droplet) the improvement level is more than 85% and for the other cases the improvements have been quantified in Figure 6c. This improvement is attributed to the implementation of the entire spectrum and accounting for the cohesive effect of the internal viscosity of droplets. To clarify the improvement of the current model compared to the original model, the percentage of residual reduction (i.e., the relative decrease in the residuals when applying two models) for the range of droplet sizes is reported in the plot. It is interesting to see that the current model provides more accurate predictions towards the smaller length scales (i.e., the dissipation subrange). The improvements level out for the scales corresponding to the internal viscosity effect. It should be noted that applying both the entire spectrum and the physical effect of internal viscosity for d_0 = 100 μm yields a very low breakup rate of 0.71 s^{-1}, whereas incorporating only the internal viscosity without the entire energy spectrum leads to the breakup rate of 2.55 s^{-1}. Figure 6d shows the separate influence of the entire energy spectrum and the internal viscosity effects on improvements to the model. The figure shows that the two terms decrease the residual reduction in a cooperative way. Close to the dissipation subrange, the application of the entire energy spectrum contributes more to residual reduction, whereas including the internal viscous effect has a greater influence on larger droplets. It can be concluded that the breakup rate obtained for the minimum droplet size verifies the assumption that the breakup outside the inertial subrange requires the entire energy spectrum and accounting for the other stresses.

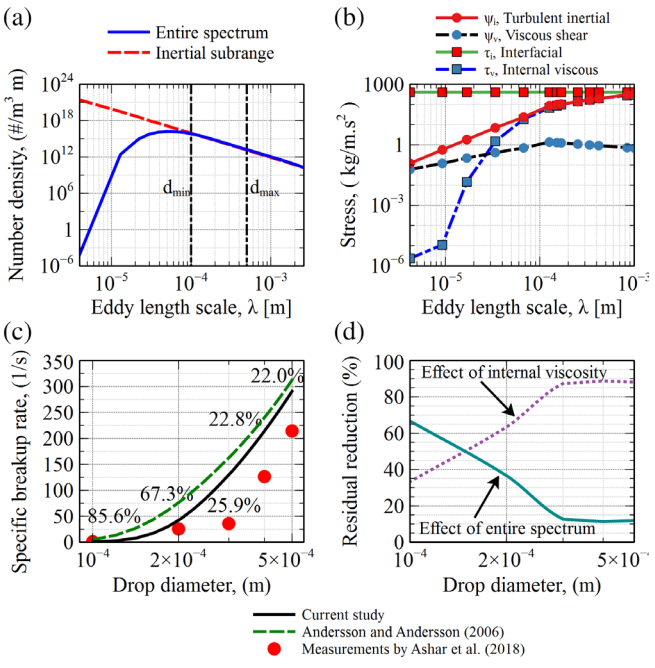

FIGURE 6 (a) Vortices number density plot, (b) stress analysis, and (c, d) validation of specific breakup rate of the experimental measurements by Ashar et al[46] [Color figure can be viewed at wileyonlinelibrary.com]

Theoretically, equating the disruptive and cohesive stresses introduced in Table 2 results in a droplet diameter that could be a representation of the maximum stable droplet size. There are, though, physical constraints that should be respected while carrying out the stress analysis. The size of the smallest vortex interacting with the droplet is limited by half of the Kolmogorov length scale, and the upper limit for the effective vortex size is λ $d_0 \leq 10$. Moreover, to ensure that the movement of a maximum stable fluid particle is controlled by the vortex motion, the third criterion was established to investigate the value of the Stokes number for the maximum allowable vortex size. The Stokes number of less than or equal to unity is required to ensure that the droplet follows the flow field streamlines. Figure 7 shows a general methodology practiced in this work to obtain the maximum stable droplet diameter using stress analysis. The three criteria mentioned were applied to find the maximum stable size for a droplet. The stress analysis results show that by decreasing the droplet size, the cohesive stresses become more dominant and surpass the summation of turbulent inertia and viscous shear stresses for the effective range of vortex sizes. The stress ratio (i.e., ψ_d/τ_c) is less than one due to the higher magnitude of stabilizing stresses; this

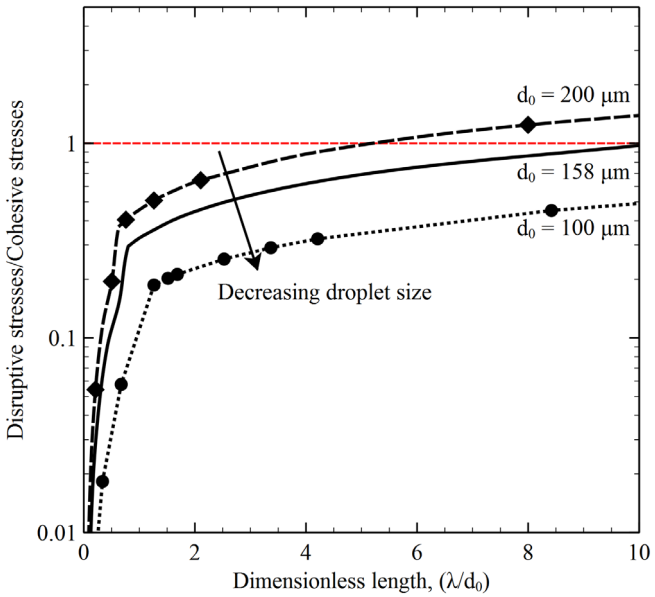

FIGURE 7 Ratio of disruptive to cohesive stresses as a function of dimensionless length scale for water–rapeseed oil system reported by Ashar et al[46] [Color figure can be viewed at wileyonlinelibrary.com]

suggests that not all the required criteria have been met to obtain the maximum stable droplet size. However, for a droplet diameter of d_0 = 158 μm, the stress ratio is approximately one for the largest acceptable vortex size ($\lambda/d_0 \approx 10$), whereas the Stokes number is 0.54 for these conditions. Therefore, it is concluded that performing the stress analysis predicts d_{max} = 158 μm as the maximum stable droplet diameter. Furthermore, the sensitivity of the results to the choice of effective vortex size was explored by assigning the upper limit (i.e., λ/d_0) as 5, 15 and 20, leading to d_{max} = 197 μm,d_{max} = 146 μm, and d_{max} = 126 μm, respectively. Equation (1) was applied to compare the prediction of the stress analysis approach with a semiempirical model. This equation was derived for the inertia dominant mechanism without the effect of dispersed phase viscosity. Calculating the maximum stable droplet diameter using Equation (1) results in d_{max} = 182 μm. The experiment shows negligible value for the breakup rate of droplet size class from 50 μm to 150 μm, with an average diameter of d_0 = 100 μm. A Comparison of different methods for the prediction of stable size shows the importance of including all the stresses for the breakup modeling and obtaining the maximum stable droplet diameter.

3.3 | Inertia and turbulent viscous stresses—dissipation subrange

This section evaluates the performance of the model for predicting the maximum stable droplet diameter, specifically when it occurs within the dissipation subrange of turbulence, and turbulent viscous stress is more important than turbulent inertia stress. To the best of our knowledge, there are no direct breakup rate measurements for turbulent systems with mother droplet diameters even close to the lower end of the dissipation subrange. However, there are experimental studies of the maximum stable droplet sizes under different operating conditions and with different fluid properties. Therefore, the validation process was adapted to account for the available experimental data. We investigated which of the stresses are more important when determining the maximum stable droplet diameter, and, consequently, two different regimes, a turbulent inertia regime and a turbulent viscous regime were distinguished.

The first set of experiments have been reported by Håkansson et al,[44] who measured the maximum droplet diameters for a high-volume fraction, and high-viscosity industrial scale water–rapeseed oil inside batch and continuous rotor stator mixers. Subsequently, the experiments were fitted to a power-law regression model with respect to the tip velocity (U_{tip}). The similarity between the exponent of the empirical expression for turbulent viscous fragmentation ($d_{stable} \propto \varepsilon^{-1/2}$) and the regression model was the basis for interpreting that the fragmentation was dominated by the turbulent viscous regime. We have selected the experimental data for tip velocities of 23 m s^{-1} and 30 m s^{-1} corresponding to the turbulent dissipation rates of 405 000 m^2 s^{-3} and 900 000 m^2 s^{-3}. The measured stable droplet diameters and Kolmogorov length scales for the two different turbulent dissipation rates were reported as, 2.6 μm, 1.7 μm, 54 μm and 39 μm, respectively. The second set of experimental data was based on Vankova et al.[39] They investigated the effect of different operating conditions, such as turbulent dissipation rate, interfacial tension, viscosity and volume fraction, on mean and maximum droplet diameters within a narrow-gap homogenizer. Several oils with different viscosities were used as the dispersed phase, and the coalescence effects were suppressed by using emulsifier. The turbulent dissipation rate was obtained from numerical simulations for two flow rates.[69] For additional flow rates Vankova et al, derived an expression based on an effective local volume, and the expression was validated with controlled emulsification experiments. Their experimental findings indicate that the values of ε quantified by the obtained expression led to close predictions of d_{max}. Table 4 shows the details of different emulsions used in the current validation study in conjunction with experiments for the stable droplet diameters and the predictions based on the stress analysis approach. The predictions were determined based on the estimation of internal viscosity for three different shapes of the deformed droplets (sphere, cylinder, ellipsoid). The letters "H" and "V" stand for the measurements reported by Håkansson et al,[44] and Vankova et al,,[39] respectively. "U23" and "U30" represent the tip velocities of 23 m s^{-1} and 30 m s^{-1}. The other abbreviations for the dispersed phase and emulsifiers are Sil: silicon oil, Bet: SDP3S + Betaine solutions, C16: hexadecane, Br: Brij 58, Min: mineral oil, SBO: soybean oil, NaC: Na caseinate. Additional details can be found in the original publications.[39,44] It should be remembered that the maximum stable size is determined by equating the disruptive and cohesive stresses for the effective size range of a turbulent structure by adopting the entire turbulent energy spectrum, while the Stokes number should be less then, or equal to, unity for the maximum vortex size. It should also be noted that for the two cases with the highest *Oh* numbers, using different shapes led to negligible effects, which emphasizes that

TABLE 4 Summary of operational conditions used to differentiate various breakup mechanisms

Emulsion abbreviation	ε (m^2s^{-3})	σ (kg s^{-2})	μ_c (kg $m^{-1}s^{-1}$)	μ_d (kg $m^{-1}s^{-1}$)	*Oh* number	d_{max} (μm) (Exp)	d_{max} (μm) (Model)[a]		
							S	C	E
H-U23	405,567	0.005	0.0877	0.149	30.8	2.7	5.1	5.1	5.1
H-U30	900,000	0.005	0.0738	0.149	36.1	1.7	3.6	3.6	3.6
V-Sil-Bet-17	439,920	0.0047	0.0179	0.095	19.2	5.4	5.4	5.8	5.5
V-Sil-Bet-15	415,710	0.0047	0.0152	0.095	18.4	5.9	5.9	7.2	6.2
V-Sil-Bet-0.7	370,000	0.0047	0.0169	0.095	19.8	6.8	5.1	7.1	6.5
V-C16-Br	180,300	0.007	0.001	0.003	0.7	5.5	3.6	3.6	3.6
V-Min-Br	266,700	0.0083	0.001	0.027	3.2	9.8	8	13.5	10.7
V-SBO-NaC	180,300	0.0205	0.001	0.05	2.7	21	17	24	19
V-Sil-Br	180,300	0.0103	0.001	0.095	6.6	13	21	33.5	27
V-Sil-Br-200	259,200	0.0117	0.001	0.22	10.4	31.4	40	57	47

[a]Abbreviations: C, cylinder; E, ellipsoid; S, sphere.

interfacial tension is the controlling cohesive stress for the breakup. However, for other cases, an ellipsoidal shape generally results in closer predictions of stable droplet diameter.

Analyzing the contributions of different stresses when obtaining the maximum stable droplet diameters, one can discern two distinct regimes for droplet breakups based on the operational conditions. Figure 8 shows the ratio of measured versus predicted maximum stable droplet diameters as a function of the dimensionless length scale (turbulent structure size over the Kolmogorov length scale). The plot shows a regime map of different breakup mechanisms for the fluid particles. The results are based on different data points covering a wide range of operational conditions for emulsion systems (e.g., 100 000 [m^2s^{-3}] < ε < 900 000 [m^2 s^{-3}]). Two distinct zones were identified by virtue of stress analysis and applying the entire turbulent energy spectrum. The first region characterizes the breakup of fluid particles due to the turbulent viscous shear stress (i.e., viscous dominant regime, $\psi_i < \psi_v$). Another feature of this regime is that the maximum stable droplet diameter occurs in sub-Kolmogorov zone ($d_{max} < \eta$) showing the importance of viscous shear stress. The second zone is where the turbulent inertia is the dominating stress for droplet breakups. In other words, the magnitude of viscous shear stress is small enough that its contribution to the breakup is negligible. In general, one can conclude from Figure 8 that the vortex of size one order of magnitude larger than the Kolmogorov length scale is the border line for the regime change. The breakup of sub-Kolmogorov droplets in the presence of turbulence is quantified by the turbulent viscous stresses, while for larger droplets (>10η), even though the turbulent viscous stress is present, the inertia is the prevailing factor for the breakup phenomenon. While Figure 8 shows a seemingly simple two blocks, each representing a breakup mechanism, it comprises a validation procedure for every data point based on evaluating the number density of vortices, stress analysis, and computing the breakup rates. As an example, Figure 9 is to clarify the validation procedure for both inertia (e.g., V-C16-Br) and viscous (e.g., H-U23) regimes.

Figure 9a,c compares the breakup rates using the new modeling framework and the original model of the Andersson and Andersson breakup rate model,[21] whereas Figure 9b,d shows the results of stress analysis for the predicted d_{max}. The breakup rate values for viscous (H-U23) and inertia (V-C16-Br) regimes show significant difference employing the two formulations. There are two key points from the breakup rates computations worth emphasizing. Applying all the stresses and the entire turbulent energy spectrum substantially revised the magnitude of breakup rates for the current model compared to the original one that Andersson and Andersson derived for the inertial subrange. Due to the lack of experimental measurements of the specific breakup rates for these cases, an explicit evaluation of the current model cannot go further. However, the main factor that differentiates the two modeling approaches is the prediction of breakup rates for the measured d_{max}. The specific breakup rates using the Andersson and Andersson model for the viscous and inertia

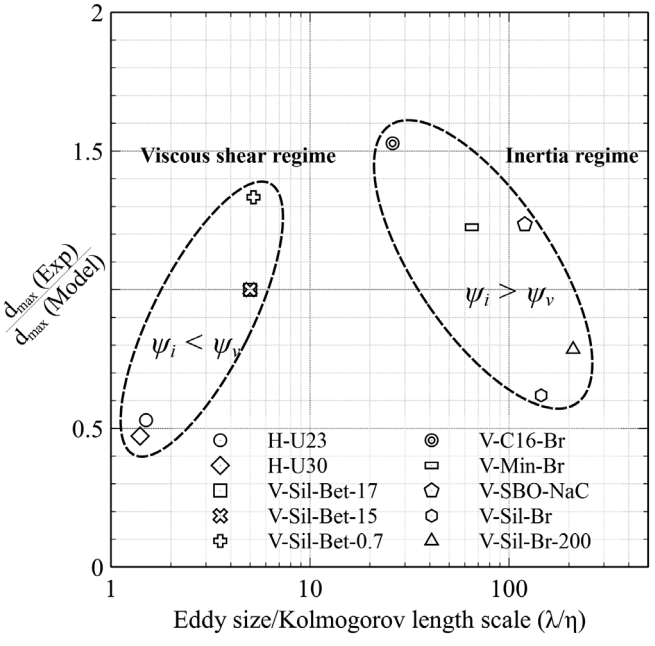

FIGURE 8 Differentiation of turbulent viscous regime and inertia regime based on stress analysis

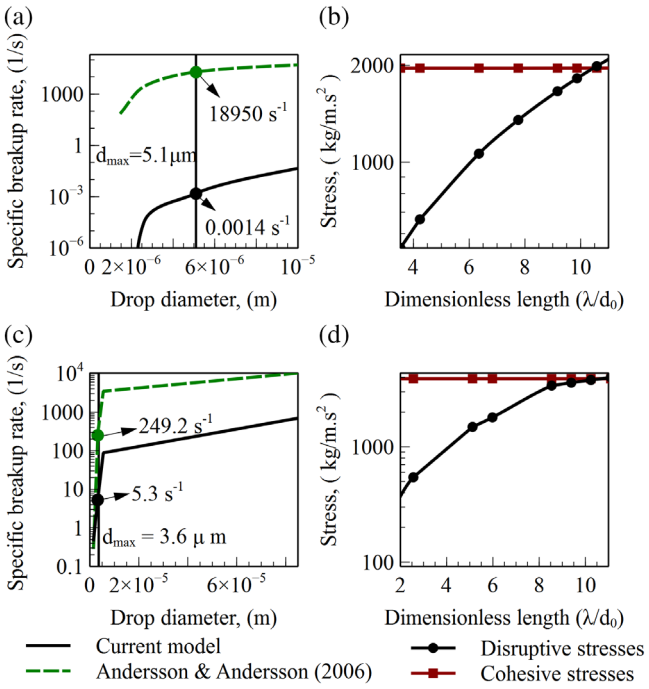

FIGURE 9 Results of breakup rates with the new model and baseline model in conjunction with stress analyses for (a, b) H-U23, and (c, d) V-C16-Br (see Table 4 for abbreviations) [Color figure can be viewed at wileyonlinelibrary.com]

dominant regimes are, 18 950 s^{-1}, and 249.2 s^{-1}, respectively. However, the corresponding values using the current model show significant improvements with lower breakup rates for the maximum stable droplet diameters (i.e., 0.0014 s^{-1} and 5.3 s^{-1}). The current modeling strategy successfully predicts the maximum stable droplet size by estimating minor breakup rates. To support this argument and underline the role of different stresses, the total disruptive and cohesive stresses were also plotted for the diameters of the maximum stable droplets (Figure 9b,d). The two plots (summation of cohesive and disruptive stresses) intersect at approximately $\lambda/d_0 \approx 10$, which additionally verifies that the modeling approach is a reliable method for determining the stable size for both inertia and viscous regimes for emulsions.

The proposed modeling formulation provides a means to obtain not only the maximum stable droplet diameter but also the specific breakup rates of droplets with diameters either smaller or larger than the Kolmogorov length scale. Analyzing the stresses for low-viscosity droplets shows that the dominant stabilizing stress is the interfacial tension of small-sized droplets, which is larger than the summation of disruptive stresses. For high viscosity droplets, the stabilizing effect of internal viscous stress should be taken into consideration. The magnitude of the viscous shear stresses is comparable and, in some cases, even larger than the turbulent inertia stresses, which emphasizes the role of this stress component in the breakup mechanism. In other words, a breakup rate model formulation that does not consider the effect of viscous shear stress will be prone to error. Therefore, applying the new breakup rate model demonstrates that, firstly, the model predicts negligible breakup rates for experimental measurements of maximum stable droplet size, which confirms the flexibility of the model for sub-Kolmogorov droplets. Secondly, the stress analysis results ensure that the influential stresses are included in breakup rate modeling.

4 | CONCLUSIONS

A new breakup rate model was developed in this work to account for the different breakup mechanisms covering the inertial and dissipation subranges of turbulence. The entire spectrum of turbulent energy was applied to evaluate the number density of vortices and the second-order structure function. Further, the model embodied all the disruptive stresses, (i.e., turbulent inertia and viscous shear), and the cohesive stresses, including interfacial tension and internal viscous stress. This is a new feature for breakup modeling, as most of the available models either neglect the influence of these stresses or require the calibration of empirical constants. The formulation of a new model enabled us to account for the transition of fluid particle breakup from inertia to the viscous regime. For droplets with a wide range of diameters stretching from the dissipation subrange to the inertial subrange, the current model differentiates the breakup mechanisms seamlessly across all size ranges. The applicability of the model for the inertial subrange was verified by comparing predictions with measurements of specific breakup rates. The validation showed that, within the inertial subrange, the model predictions are similar to the baseline model.[21] For the transition region between the inertial to dissipation subrange, the model showed good improvement in predicting the breakup rates for the entire size interval of droplets. The separate effects of the entire energy spectrum and the internal viscosity on model improvements were also presented. The model was validated toward the low end of the dissipation subrange by comparing predictions of d_{max} with experimental data. In order to account for the deformed shape of viscous droplets in computing, the internal viscous stress of three different shapes, sphere, cylinder and ellipsoid, were utilized. The model successfully predicted the maximum stable droplet sizes obtained by including the entire turbulent energy spectrum and stress analysis. The model provided more realistic predictions for this subrange of turbulence and showed that any attempts to improve the breakup kernels of emulsions require the incorporation of all the stresses and the entire spectrum of turbulent energy; otherwise, the approach will be prone to error by several orders of magnitude. A regime map for different breakup mechanisms that takes into account the length scales of vortices was also established. The model was validated for a range of dissipation rates that run from the minimum value of 8.5 (m^2 s^{-3}) to the maximum value of 9×10^5 (m^2 s^{-3}). Nevertheless, outside this range, the model requires validations. Further, the model is tested under *Oh* range of 0.01–36, and potentially for higher values *Oh* > 100 validation is required. Individual model components can also be further evaluated. For instance, the second-order structure function should be validated to verify its

application in future kernel developments. The structure function was implicitly validated through its application in the current breakup rate model. As the model filters out the effective size range of eddies, the integration limits can be limited to the length scales with the greatest contribution to the breakup. This could reduce the overall computational efforts.

The developed modeling framework conceptualizes the possibility of different mechanisms for the breakup. It retains the breakup rates for a truly inertia-dominant breakup phenomenon, while it improves predictions close to the border of the inertial and dissipation subrange of turbulence. The major contributions of this work can be outlined as below:

- The proposed model differentiates the inertia and viscous regimes as breakup mechanisms through stress analysis.
- The breakup rate model utilizes no tunable parameters with respect to the disruptive and cohesive stress criteria applied, neither is the model sensitive to the integration limits. On the other hand, selection of different turbulent model terms influences the model predictions.
- Effects of all disruptive and cohesive stresses are included for breakup rate predictions, allowing the estimation of the maximum stable droplet diameter.
- The model is capable of predicting breakup rates for sub-Kolmogorov droplets by recognizing the importance of the entire energy spectrum and internal viscosity.
- The model validations for inertial subrange, transition zone and dissipation subrange showed that the model considers the prominent breakup properties of different regions.

ACKNOWLEDGMENT

Financial support from the Swedish Research Council (Grant: 621-2013-5964) is acknowledged.

NOTATION

c_η	model parameter for nondimensional cut-off function for energy dissipation subrange (–)
c_L	model parameter for nondimensional cut-off function for energy containing subrange (–)
d_0	mother droplet diameter (m)
d_{max}	maximum stable droplet diameter (m)
$E(\kappa)$	energy spectrum ($m^3\ s^{-2}$)
F	hypergeometric function (–)
$f_L(2\pi/\lambda L)$	nondimensional cut-off function for energy containing subrange (–)
$f_\eta(2\pi/\lambda\eta)$	nondimensional cut-off function for energy dissipation subrange (–)
$\bar{G}$	local deformation rate (s^{-1})
K	Bessel function (–)
k	turbulent kinetic energy ($m^2\ s^{-2}$)
L	integral length scale (m)
$\dot{n}_\lambda$	number density of vortices per unit volume (m^{-4})
Oh	Ohnesorge number (–)
P	breakup probability (–)
p_0	model constant (–)
Re_λ	Taylor-scale Reynolds number (–)
Re_L	integral scale Reynolds number (–)
$T_1 \dots T_5$	functions for analytical solution of structure function (–)
t_i	breakup timescale (s)
u_λ	mean velocity fluctuation ($m\ s^{-1}$)
β	model constant (–)
Γ	gamma function (–)
λ	vortex length scale (m)
$\langle[\delta v]^2\rangle(\lambda)$	second-order longitudinal structure function ($m^2\ s^{-2}$)
ε	turbulent dissipation rate ($m^2\ s^{-3}$)
η	Kolmogorov length scale (m)
μ_c, μ_d	dynamic viscosity of continuous and dispersed phases (Pa s)
ν_c	kinematic viscosity ($m^2\ s^{-1}$)
ρ_c, ρ_d	density of continuous and dispersed phases ($kg\ m^{-3}$)
σ	interfacial tension ($kg\ s^{-2}$)
τ_c	total cohesive stress ($kg\ m^{-1}\ s^{-2}$)
τ_{ext}	external stress ($kg\ m^{-1}\ s^{-2}$)
τ_i	interfacial stress ($kg\ m^{-1}\ s^{-2}$)
τ_v	internal viscous stress ($kg\ m^{-1}\ s^{-2}$)
χ_{energy}	energy criterion (–)
χ_{stress}	stress criterion (–)
ψ_d	total disruptive stress ($kg\ m^{-1}\ s^{-2}$)
ψ_i	turbulent inertial stress ($kg\ m^{-1}\ s^{-2}$)
ψ_v	viscous shear stress ($kg\ m^{-1}\ s^{-2}$)
$\dot{\omega}$	interaction frequency (s^{-1})
Ω_s	breakup rate (s^{-1})

ORCID

Mohsen Karimi https://orcid.org/0000-0002-1182-1133

REFERENCES

1. Ramkrishna D. *Population Balances: Theory and Applications to Particulate Systems in Engineering*. 1st ed. San Diego, CA: Academic Press; 2000.
2. Marchisio DL, Fox R. *Computational Models for Polydisperse Particulate and Multiphase Systems*. Cambridge: Cambridge University Press; 2013.
3. Rayleigh L. On the stability, or instability, of certain fluid motions. *Proc Lond Math Soc*. 1879;X:57-72.
4. Taylor GI. The viscosity of a fluid containing small drops of another fluid. *Proc R Soc Lond A*. 1932;138:41-48. https://doi.org/10.1098/rspa.1932.0169.
5. Taylor GI. The formation of emulsions in definable fields of flow. *Proc R Soc A Math Phys Eng Sci*. 1934;146(858):501-523. https://doi.org/10.1098/rspa.1934.0169.
6. Hinze JO. Fundamentals of the hydrodynamic mechanism of splitting in dispersion processes. *AIChE J*. 1955;1(3):289-295. https://doi.org/10.1002/aic.690010303.
7. Prince MJ, Blanch HW. Bubble coalescence and break-up in air-sparged bubble columns. *AIChE J*. 1990;36(10):1485-1499. https://doi.org/10.1002/aic.690361004.

8. Rodríguez-Rodríguez J, Martínez-Bazán C, Montañes JL. A novel particle tracking and break-up detection algorithm: application to the turbulent break-up of bubbles. *Meas Sci Technol*. 2003;14(8):1328-1340. https://doi.org/10.1088/0957-0233/14/8/319.
9. Martínez-Bazán C, Rodríguez-Rodríguez J, Deane GB, Montaes JL, Lasheras JC. Considerations on bubble fragmentation models. *J Fluid Mech*. 2010;661:159-177. https://doi.org/10.1017/S0022112010003186.
10. Wieringa JA, Van Dieren F, Janssen JJM, Agterof WGM. Droplet breakup mechanisms during emulsification in colloid mills at high dispersed phase volume fraction. *Chem Eng Res Des*. 1996;74(5):554-562.
11. Janssen JMH, Meijer HEH. Droplet breakup mechanisms: stepwise equilibrium versus transient dispersion. *J Rheol*. 1993;37(4):597-608. https://doi.org/10.1122/1.550385.
12. Janssen JJM, Boon A, Agterof WGM. Influence of dynamic interfacial properties on droplet breakup in simple shear flow. *AIChE J*. 1994;40(12):1929-1939.
13. Scarbolo L, Bianco F, Soldati A. Coalescence and breakup of large droplets in turbulent channel flow. *Phys Fluids*. 2015;27:73302. https://doi.org/10.1063/1.4923424.
14. Perlekar P, Biferale L, Sbragaglia M, Srivastava S, Toschi F. Droplet size distribution in homogeneous isotropic turbulence. *Phys Fluids*. 2012;24:65101. https://doi.org/10.1063/1.4719144.
15. Coulaloglou CA, Tavlarides LL. Description of interaction processes in agitated liquid–liquid dispersions. *Chem Eng Sci*. 1977;32(11):1289-1297. https://doi.org/10.1016/0009-2509(77)85023-9.
16. Luo H, Svendsen HF. Theoretical model for drop and bubble breakup in turbulent dispersions. *AIChE J*. 1996;42(5):1225-1233. https://doi.org/10.1002/aic.690420505.
17. Tsouris C, Tavlarides LL. Breakage and coalescence models for drops in turbulent dispersions. *AIChE J*. 1994;40(3):395-406. https://doi.org/10.1002/aic.690400303.
18. Konno M, Matsunaga Y, Arai K, Saito S. Simulation model for breakup process in an agitated tank. *J Chem Eng Japan*. 1980;13(1):67-73. https://doi.org/10.1252/jcej.13.67.
19. Lee C-H, Erickson LE, Glasgow LA. Bubble breakup and coalescence in turbulent gas–liquid dispersions. *Chem Eng Commun*. 1987;59(1–6):65-84. https://doi.org/10.1080/00986448708911986.
20. Alopaeus V, Koskinen J, Keskinen KI, Majander J. Simulation of the population balances for liquid–liquid systems in a nonideal stirred tank. Part 2-parameter fitting and the use of the multiblock model for dense dispersions. *Chem Eng Sci*. 2002;57(10):1815-1825. https://doi.org/10.1016/S0009-2509(02)00067-2.
21. Andersson R, Andersson B. Modeling the breakup of fluid particles in turbulent flows. *AIChE J*. 2006;52(6):2031-2038. https://doi.org/10.1002/aic.
22. Han L, Liu Y. A theoretical model for droplet breakup in turbulent dispersions. *Chem Eng Sci*. 2011;66(4):766-776. https://doi.org/10.1016/j.ces.2010.11.041.
23. Xing C, Wang T, Guo K, Wang J. A unified theoretical model for breakup of bubbles and droplets in turbulent flows. *AIChE J*. 2015;61(4):1391-1403. https://doi.org/10.1002/aic.14709.
24. Lasheras JC, Eastwood C, Martinez-Bazen C, Montaes JL. A review of statistical models for the break-up an immiscible fluid immersed into a fully developed turbulent flow. *Int J Multiph Flow*. 2002;28(2):247-278. https://doi.org/10.1016/S0301-9322(01)00046-5.
25. Liao Y, Lucas D. A literature review of theoretical models for drop and bubble breakup in turbulent dispersions. *Chem Eng Sci*. 2009;64(15):3389-3406. https://doi.org/10.1016/j.ces.2009.04.026.
26. Solsvik J, Tangen S, Jakobsen HA. On the constitutive equations for fluid particle breakage. *Rev Chem Eng*. 2013;29(5):241-356. https://doi.org/10.1515/revce-2013-0009.
27. Bałdyga J, Podgorska W. Drop break-up in intermittent turbulence: maximum stable and transient sizes of drops. *Can J Chem Eng*. 1998;76(1):456-470. https://doi.org/10.1002/cjce.5450760316.
28. Shinnar R. On the behaviour of liquid dispersions in mixing vessels. *J Fluid Mech*. 1961;10(2):259-275. https://doi.org/10.1017/S0022112061000214.
29. Håkansson A, Trägårdh C, Bergenståhl B. Dynamic simulation of emulsion formation in a high pressure homogenizer. *Chem Eng Sci*. 2009;64(12):2915-2925. https://doi.org/10.1016/J.CES.2009.03.034.
30. Solsvik J, Skjervold VT, Han L, Luo H, Jakobsen HA. A theoretical study on drop breakup modeling in turbulent flows: the inertial subrange versus the entire spectrum of isotropic turbulence. *Chem Eng Sci*. 2016;149:249-265. https://doi.org/10.1016/j.ces.2016.04.037.
31. Solsvik J, Jakobsen HA. Development of fluid particle breakup and coalescence closure models for the complete energy spectrum of isotropic turbulence. *Ind Eng Chem Res*. 2016;55(5):1449-1460. https://doi.org/10.1021/acs.iecr.5b04077.
32. Solsvik J, Jakobsen HA. A review of the statistical turbulence theory required extending the population balance closure models to the entire spectrum of turbulence. *AIChE J*. 2016;62(5):1795-1820. https://doi.org/10.1002/aic.
33. Karimi M, Andersson R. An exploratory study on fluid particles breakup rate models for the entire spectrum of turbulent energy. *Chem Eng Sci*. 2018;192:850-863. https://doi.org/10.1016/j.ces.2018.08.016.
34. Davies JT. Drop sizes of emulsions related to turbulent energy dissipation rates. *Chem Eng Sci*. 1985;40(5):839-842. https://doi.org/10.1016/0009-2509(85)85036-3.
35. Calabrese RV, Chang TPK, Dang PT. Drop breakup in turbulent stirred tank contactors. Part I: effect of dispersed phase viscosity. *AIChE J*. 1986;32(4):657-666. https://doi.org/10.1002/aic.690320416.
36. Chen HT, Middleman S. Drop size distribution in agitated liquid–liquid systems. *AIChE J*. 1967;13(5):989-995.
37. Padron Aldana GA. *Effect of Surfactants on Drop Size Distributions in a Batch, Rotor-Stator Mixer*. PhD dissertation, University of Maryland, College Park. 2004.
38. Arai K, Konno M, Matunaga Y, Saito S. Effect of dispersed-phase viscosity on the maximum stable drop size for breakup in turbulent flow. *J Chem Eng Japan*. 1977;10(4):325-330. https://doi.org/10.1252/jcej.10.325.
39. Vankova N, Tcholakova S, Denkov ND, Ivanov IB, Vulchev VD, Danner T. Emulsification in turbulent flow. 1. Mean and maximum drop diameters in inertial and viscous regimes. *J Colloid Interface Sci*. 2007;312(2):363-380. https://doi.org/10.1016/j.jcis.2007.03.059.
40. Berkam PD, Calabrese RV. Dispersion of viscous fluids by turbulent flow in a static mixer. *AIChE J*. 1988;34(4):602-609.
41. Carrillo De Hert S, Rodgers TL. On the effect of dispersed phase viscosity and mean residence time on the droplet size distribution for high-shear mixers. *Chem Eng Sci*. 2017;172:423-433. https://doi.org/10.1016/j.ces.2017.07.002.
42. Ramezani M, Legg MJ, Haghighat A, Li Z, Vigil RD, Olsen MG. Experimental investigation of the effect of ethyl alcohol surfactant on oxygen mass transfer and bubble size distribution in an air–water multiphase Taylor-Couette vortex bioreactor. *Chem Eng J*. 2017;319:288-296. https://doi.org/10.1016/j.cej.2017.03.005.
43. Boxall JA, Koh CA, Sloan ED, Sum AK, Wu DT. Droplet size scaling of water-in-oil emulsions under turbulent flow. *Langmuir*. 2012;28(1):104-110. https://doi.org/10.1021/la202293t.
44. Håkansson A, Chaudhry Z, Innings F. Model emulsions to study the mechanism of industrial mayonnaise emulsification. *Food Bioprod Process*. 2016;98:189-195. https://doi.org/10.1016/j.fbp.2016.01.011.
45. Tikhomirov VM. In: Tikhomirov VM, ed. *Selected Works of a. N. Kolmogorov*. 25th ed. Dordrecht: Springer Science & Business Media; 1991. https://doi.org/10.1007/978-94-011-3030-1.
46. Ashar M, Arlov D, Carlsson F, Innings F, Andersson R. Single droplet breakup in a rotor-stator mixer. *Chem Eng Sci*. 2018;181:186-198. https://doi.org/10.1016/j.ces.2018.02.021.

47. Batchelor GK. *The Theory of Homogeneous Turbulence*. Cambridge: Cambridge University Press; 1953.
48. Pope SB. *Turbulent Flows*. 1. Cambridge: Cambridge University Press; 2000. doi:https://doi.org/10.1088/0957-0233/12/11/705.
49. Jakobsen HA. *Chemical Reactor Modeling Multiphase Reactive Flows*. 2nd ed. Switzerland: Springer International Publishing; 2014. doi:https://doi.org/10.1007/978-3-319-05092-8.
50. Eastwood CD, Armi L, Lasheras JC. The breakup of immiscible fluids in turbulent flows. *J Fluid Mech*. 2004;502(2004):309-333. https://doi.org/10.1017/S0022112003007730.
51. Han L, Gong S, Ding Y, Fu J, Gao N, Luo H. Consideration of low viscous droplet breakage in the framework of the wide energy spectrum and the multiple fragments. *AIChE J*. 2015;61(7):2147-2168. https://doi.org/10.1002/aic.
52. Han L, Gong S, Li Y, et al. A novel theoretical model of breakage rate and daughter size distribution for droplet in turbulent flows. *Chem Eng Sci*. 2013;102:186-199. https://doi.org/10.1016/j.ces.2013.06.046.
53. Andersson R, Andersson B. On the breakup of fluid particles in turbulent flow. *AIChE J*. 2006;52(6):2020-2030. https://doi.org/10.1002/aic.
54. Ghasempour F, Andersson R, Andersson B. Multidimensional turbulence spectra—statistical analysis of turbulent vortices. *App Math Model*. 2014;38:4226-4237.
55. Ghasempour F, Andersson R, Andersson B. Number density of turbulent vortices in the entire energy spectrum. *AIChE J*. 2014;60(11):3989-3995. https://doi.org/10.1002/aic.14622.
56. Ghasempour F, Andersson R, Andersson B. Identification and characterization of three-dimensional turbulent flow structures. *AIChE J*. 2016;62(4):1265-1277. https://doi.org/10.1002/aic.
57. Solsvik J. Turbulence modeling in the wide energy spectrum: explicit formulas for Reynolds number dependent energy spectrum parameters. *Eur J Mech B/Fluids*. 2017;61:170-176. https://doi.org/10.1016/j.euromechflu.2016.10.011.
58. Solsvik J, Jakobsen HA. A review of the concepts for deriving the equations of change from the classical kinetic theory of gases: single-component, multicomponent, and reactive gases. *Eur J Mech B/Fluids*. 2016;56:46-65. https://doi.org/10.1016/j.euromechflu.2015.11.005.
59. Ghasempour F, Andersson R, Kevlahan N, Andersson B. Multidimensional turbulence spectra—identifying properties of turbulent structures. *J Phys Conf Ser*. 2011;318(Section 4):1-11. https://doi.org/10.1088/1742-6596/318/4/042022.
60. Davidson PA. *Turbulence: An Introduction for Scientists and Engineers*. Oxford: Oxford University Press; 2004.
61. Sawford BL, Hunt JCR. Effects of turbulence structure, molecular diffusion and source size on scalar fluctuations in homogeneous turbulence. *J Fluid Mech*. 1986;165:373-400. https://doi.org/10.1017/S0022112086003142.
62. Andersson R, Helmi A. Computational fluid dynamics simulation of fluid particle fragmentation in turbulent flows. *App Math Model*. 2014;38(17–18):4186-4196. https://doi.org/10.1016/j.apm.2014.01.005.
63. Kuboi R, Komasawa I, Otake T. Behavior of dispersed particles in turbulent liquid flow. *J Chem Eng Japan*. 1972;5(4):349-355. https://doi.org/10.1252/jcej.5.349.
64. Chen Z, Prüss J, Warnecke H. A population balance model for disperse systems: drop size distribution in emulsion. *Chem Eng Sci*. 1998;53(5):1059-1066. https://doi.org/10.1016/S0009-2509(97)00328-X.
65. Becker PJ, Puel F, Jakobsen HA, Sheibat-Othman N. Development of an improved breakage kernel for high dispersed viscosity phase emulsification. *Chem Eng Sci*. 2014;109:326-338. https://doi.org/10.1016/j.ces.2014.02.008.
66. Håkansson A, Mortensen HH, Andersson R, Innings F. Experimental investigations of turbulent fragmenting stresses in a rotor-stator mixer. Part 1. Estimation of turbulent stresses and comparison to breakup visualizations. *Chem Eng Sci*. 2017;171:625-637. https://doi.org/10.1016/j.ces.2017.06.042.
67. Håkansson A, Andersson R, Mortensen HH, Innings F. Experimental investigations of turbulent fragmenting stresses in a rotor-stator mixer. Part 2. Probability distributions of instantaneous stresses. *Chem Eng Sci*. 2017;171:638-649. https://doi.org/10.1016/j.ces.2017.06.038.
68. Shao J, Tu D. *The Jackknife and Bootstrap*. Springer, New York, NY; 1995. doi:https://doi.org/10.1007/b98966.
69. Steiner H, Teppner R, Brenn G, Vankova N, Tcholakova S, Denkov N. Numerical simulation and experimental study of emulsification in a narrow-gap homogenizer. *Chem Eng Sci*. 2006;61(17):5841-5855. https://doi.org/10.1016/j.ces.2006.04.016.

SUPPORTING INFORMATION

Additional supporting information may be found online in the Supporting Information section at the end of this article.

How to cite this article: Karimi M, Andersson R. Dual mechanism model for fluid particle breakup in the entire turbulent spectrum. *AIChE J*. 2019;65:e16600. https://doi.org/10.1002/aic.16600